frontiers in Earth Science

ORIGINAL RESEARCH
published: 17 July 2020
doi: 10.3389/feart.2020.00300

High Potency of Volcanic Contribution to the ∼400 kyr Sedimentary Magnetic Record in the Northwest Pacific

Ji Young Shin[1], Wonnyon Kim[1] and Kiseong Hyeong[2]*

[1] Deep-Sea and Seabed Mineral Resource Research Center, Korea Institute of Ocean Science and Technology, Busan, South Korea, [2] Global Ocean Research Center, Korea Institute of Ocean Science and Technology, Busan, South Korea

As the northwest Pacific has been subject to varying terrigenous input linked to paleoclimate change, the concentration of magnetic minerals in deep-sea sediments is often utilized as a proxy to reconstruct the past atmospheric circulation in the Northern hemisphere. Volcanic materials account for a significant portion of the terrigenous input, but their contribution to sedimentary magnetic properties has not been carefully investigated. This study reveals the magnetic contribution and characteristics of volcanic materials, based on particle-size specific magnetic measurements on sediments that span the last 400 kyr for five size-fractions, including ranges typically attributed to fine eolian (<2 and 2–8 μm) and coarse volcanic (8–31 and 31–63 μm) sediments. Such detrital origins were confirmed by SEM observations. Magnetic concentration (i.e., saturation isothermal remanent magnetization) of the coarse fractions is found to have a positive relationship with bulk values, making up a 23–68% portion. The volcanic contribution is more pronounced on the concentration of hard (>100 mT) magnetic minerals, showing an increased portion of 32–74%. From coercivity spectra analysis, the coarse volcanic fractions are characterized by an abundance of the ∼100 mT coercivity minerals, which can result in an increased average coercivity of bulk sediments. Around the study area, magnetic susceptibility records show synchronized variations with volcanic proportions in terrigenous sediments, validating their close relationship. Consequently, our results indicate that volcanic materials have a high potency of magnetic concentration, which can control bulk sedimentary signals in the northwest Pacific.

Keywords: volcanic materials, terrigenous input, particle size fraction, magnetic concentration, northwest Pacific

OPEN ACCESS

Edited by:
Myriam Kars,
Kôchi University, Japan

Reviewed by:
Qingsong Liu,
Chinese Academy of Sciences (CAS), China
Brendan Thomas Reilly,
University of California, San Diego, United States

****Correspondence:***
Wonnyon Kim
wkim@kiost.ac.kr

Specialty section:
This article was submitted to Geomagnetism and Paleomagnetism, a section of the journal Frontiers in Earth Science

Received: *07 May 2020*
Accepted: *26 June 2020*
Published: *17 July 2020*

Citation:
Shin JY, Kim W and Hyeong K (2020) High Potency of Volcanic Contribution to the ∼400 kyr Sedimentary Magnetic Record in the Northwest Pacific. Front. Earth Sci. 8:300. doi: 10.3389/feart.2020.00300

INTRODUCTION

Mineral dust in the North Pacific, including iron oxides, is transported mainly from the Asian inland by westerly winds (Rea et al., 1998). In agreement with the geochemical behaviors of mineral dust, the physical properties of magnetic particles (e.g., concentration and composition) in deep-sea sediments have shown long-term dependence on Cenozoic global cooling. For example, an increased concentration of magnetic minerals in sediments, particularly of high coercivity minerals

(e.g., hematite), has been an indicator of the intensified Asian dust input by source aridification (e.g., Yamazaki and Ioka, 1997; Bailey et al., 2011; Zhang et al., 2018). On orbital timescales, magnetic mineral concentration in North Pacific sediments shows a good correlation with the global oxygen isotope stack (e.g., LR04; Lisiecki and Raymo, 2005) during the Pleistocene, with its decrease or increase during colder or warmer periods, respectively (e.g., Yamazaki, 1999; Yamamoto et al., 2007; Kars et al., 2017). As an explanation for the cyclicity of the magnetic concentration, various factors have been suggested: glacial enhancement of dust input with high coercivity minerals (Doh et al., 1988), fossilized biogenic magnetite contribution relative to dust input (Yamazaki, 2009), and non-steady state diagenesis with glacial magnetite dissolution (Korff et al., 2016; Shin et al., 2018). However, the relationship between terrigenous input and magnetic concentration in orbital timescales is still unclear.

In the northwest Pacific, the atmospheric transport of volcanic materials from nearby arcs (e.g., Japan and the Kurile Islands) makes a vital part of terrigenous input (Nakai et al., 1993). The geochemical isotopic composition of terrigenous sediments provides a simple binary mixing feature between eolian and volcanic components (Pettke et al., 2000; Bory et al., 2003; Chen et al., 2007). Volcanic materials generally comprise more than 10–30 percentages of terrigenous input in the northwest Pacific (e.g., Nakai et al., 1993; Serno et al., 2014). Most magnetic studies on volcanic materials have identified that intercalated tephra layers in northwest Pacific sediments are characterized by strong magnetization (e.g., Yamamoto et al., 2007; Korff et al., 2016). In addition, a good relationship between magnetic signal and volcanic ash contribution during the last ∼800 kyr has been reported from abyssal sediments at a western marginal site (Urbat and Pletsch, 2003).

The development of methods to unmix magnetic signals helps discriminate magnetic mineral assemblages in bulk sediments, such as detrital/biogenic magnetite and hematite (e.g., Kruiver and Passier, 2001; Egli et al., 2010; Heslop, 2015). The magnetic contribution of biogenic magnetite, which significantly contributes to the bulk magnetic signals of northwest Pacific sediments, is readily decomposed by its non-interacting magnetic signature, such as a low and narrow coercivity distribution (Roberts et al., 2000; Egli, 2004). Meanwhile, detrital magnetite and hematite can be identified by a broader spectrum and their intrinsic coercivity (Egli, 2004). However, it is often difficult to decompose detrital magnetic minerals of different origins, such as eolian and volcanic components, from bulk magnetic signals. In this case, the combination of physical particle size separation and magnetic measurements provide useful insight to sediment transport mechanisms linked to particle size distribution (e.g., Bailey et al., 2011; Hatfield, 2014; Hatfield et al., 2017). In this study, the particle size separation approach is applied to isolate the magnetic properties of northwest Pacific sediments. From the particle size-dependent magnetic properties, we investigate the magnetic contribution of volcanic materials and its relationship with the climate-related magnetic variations since 400 ka.

MATERIALS AND METHODS

Materials

Sediment samples were taken from the core NPGP1302-1B (32°17.550N, 158°13.570E; **Figure 1**) on the South High of the Shatsky Rise studied by Shin et al. (2018). Terrigenous sediments of the Shatsky Rise area are mainly composed of eolian dust from Asian deserts (e.g., the Taklimakan and Gobi deserts) and volcanic materials from the nearby Japanese arcs (Natland, 1993; Zhao et al., 2006). In terms of magnetic minerals, the terrigenous fractions have experienced post-depositional alteration (i.e., magnetite dissolutions) during glacial periods, as indicated by abruptly reduced magnetizations in glacial-stage sediments (Korff et al., 2016; Shin et al., 2018). For the studied core, Shin et al. (2018) reported that magnetic minerals experienced weak alteration during Marine Isotope Stage (MIS) 2 and severe dissolution during MIS 6, 8, and 10.

To identify particle size dependence on rock magnetic properties, 20 bulk sediment samples were selected from core NGP1302-1B and physically separated into five particle size fractions (<2, 2–8, 8–31, 31–63, and >63 μm). Sample selection was based on sediment ages of NPGP1302-1B (Shin et al., 2018), covering periods of MIS 1–10. Shin et al. (2018) constructed the sediment age model through correlations of magnetic susceptibility and Ba/Ti (Ba/Al) records with adjacent cores. Radiocarbon dates spanning the last ∼20 kyr were also combined. From a total of 23 age–depth points, the average sedimentation rate was calculated as 1.60 cm/kyr, with the bottom age of 394 ka at 603 cm depth.

Particle Size Separation

Particle size separation was made following the Atterberg method (Atterberg, 1912). A bulk sediment sample of ∼2.5 g dry weight was mixed with 25 ml of a 2% Calgon solution (sodium hexametaphosphate) and distilled water and stirred sufficiently. The >63 μm fraction was extracted by sieving. Next, the sediment solution was separated into four size-fractions on the basis of Stroke's Law, in sequence from coarse to fine fractions (31–63, 8–31, 2–8, and <2 μm), by siphoning suspended sediments after deposition time of respective particle size fractions. The extraction process of each fraction was repeated at least twice to obtain purer particle size fractions. The size-separated samples were oven-dried at a temperature of ∼50°C and measured as dry masses. For the <2 μm fraction, the mass of Calgon was corrected.

Magnetic Measurements

For a total of 100 size-fractionated samples, concentration-related magnetic parameters were measured: saturation isothermal remanent magnetization (SIRM), anhysteretic remanent magnetization (ARM), and backward IRM at 100 and 300 mT in the opposite direction to the SIRM (IRM_{-100mT} and IRM_{-300mT}, respectively). Hard IRMs (HIRMs) were calculated as follows: $HIRM_{100} = 0.5 \times (SIRM + IRM_{-100mT})$ and $HIRM_{300} = 0.5 \times (SIRM + IRM_{-300mT})$.

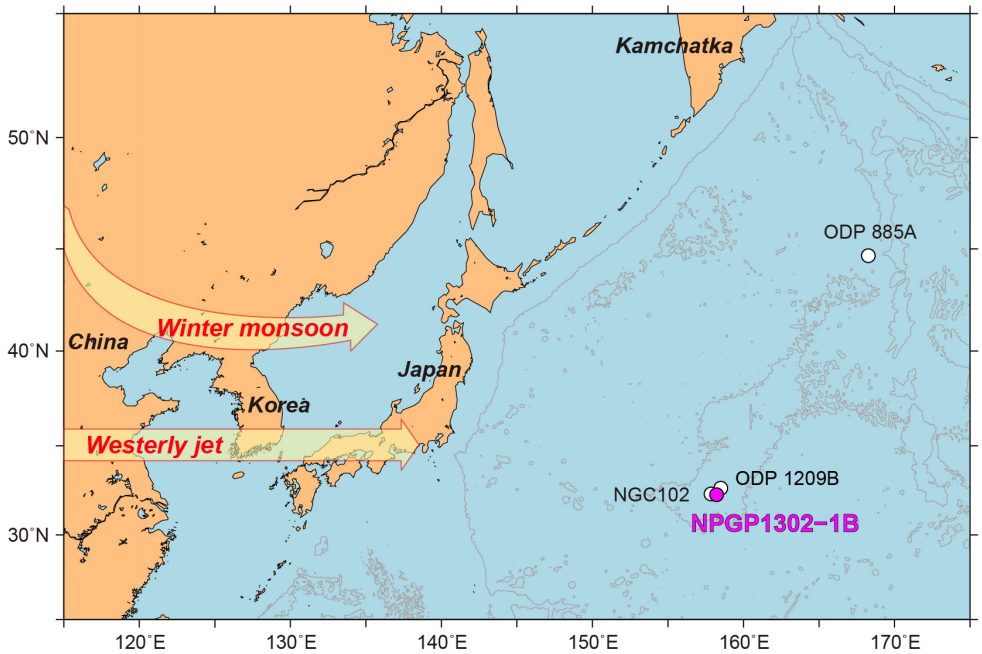

FIGURE 1 | A map showing the location of the studied core NPGP1302-1B. Cores referred in this study are also shown. In the North Pacific, eolian dust and volcanic materials are transported by the Westerly jet and the East Asian winter monsoon (yellow shaded arrows).

SIRM and ARM represent magnetizations of all grains and fine-grained ferrimagnetic minerals (e.g., magnetite), respectively (Evans and Heller, 2003). $HIRM_{100}$ and $HIRM_{300}$ reflect concentrations of magnetic minerals with >100 mT (e.g., partially oxidized magnetite) and >300 mT coercivities (e.g., hematite), respectively. S-ratios (S_{100} and S_{300}) were calculated using $S_{100} = 0.5 \times (1 - IRM_{-100mT}/SIRM)$ and $S_{300} = 0.5 \times (1 - IRM_{-300mT}/SIRM)$. S_{100} and S_{300} are applied to estimate the relative significance of magnetic minerals with <100 mT and <300 mT coercivities, respectively, among all magnetic minerals (Evans and Heller, 2003). All remanent magnetization values were measured using a Agico JR-6A spinner magnetometer.

For selected size-fractionated samples, IRM acquisition and backfield demagnetization curves were obtained using a Princeton MicroMag 3900 vibrating sample magnetometer in the Center for Advanced Marine Core Research, Kochi University, Japan. IRMs were acquired by applying DC fields of up to 1 T, with 140 nonlinear field steps. From stepwise backfield IRM demagnetization, remanence coercivity (B_{cr}) was estimated as the field reduced the remanence to zero. Based on IRM acquisition behavior, principal component analysis on coercivity distribution was performed using a fitting program (Kruiver and Passier, 2001).

Electron Microscope Observations

Scanning electron microscopy (SEM) observations were carried out for magnetic mineral extracts from selected size-fractionated samples and a volcanic ash layer. After magnetic measurements, samples were dispersed into distilled water under ultrasonication for 5 min. The sediment solution was slowly dropped into a glass vial filled with distilled water, and magnetic minerals were extracted by a rare earth magnet of 1 T which was placed next to the vial. This procedure was repeated several times to gather purer magnetic extracts. The extracted samples were dried at ~50°C in an oven overnight. Finally, the dried magnetic extracts were mounted using a carbon tape, and then coated with carbon. SEM observations were performed with a JEOL analytical field emission SEM (JSM-7610F) coupled with energy dispersive X-ray spectroscopy (EDS) at Gyeongsang National University, South Korea.

RESULTS

Magnetic concentration parameters (SIRM, ARM, $HIRM_{100}$, and $HIRM_{300}$) of size-fractionated samples were normalized by mass, and then multiplied by each mass fraction (f); representing mass-normalized and mass-weighted values, respectively. The mass-normalized values are generally higher in coarser fractions which take small portions in total mass (**Supplementary Figure S1**), indicating higher magnetic concentration. In order to take account into mass contribution together, the mass-weighted values were adopted in this study (**Figure 2**) and relative abundance of magnetic minerals in each size fraction was evaluated (e.g., Razik et al., 2014). By normalizing the mass-weighted values with bulk values, the percentage magnetic contribution (PMC) was also calculated.

The calculated parameters for the sized fractions in this study are compared with the results obtained from bulk samples in

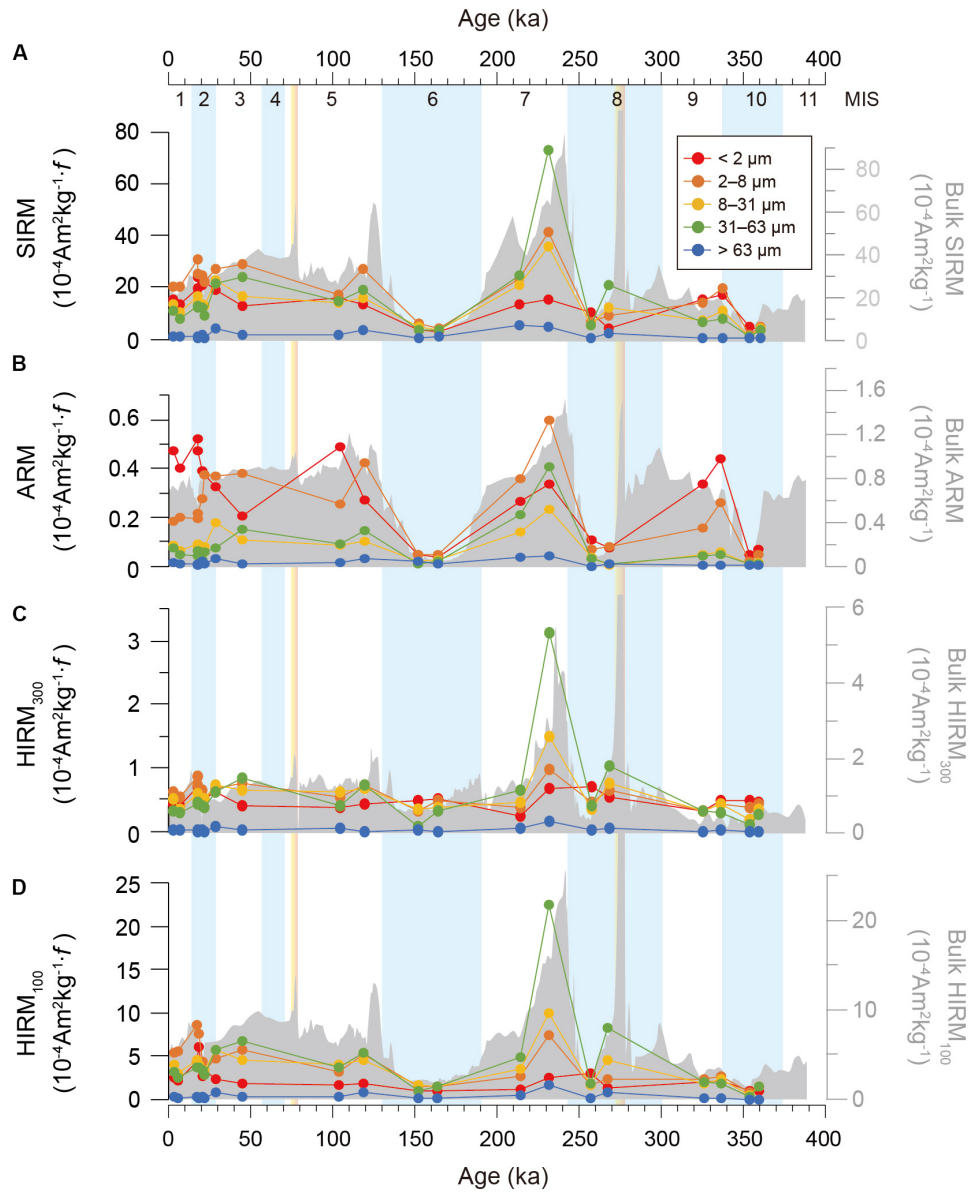

FIGURE 2 | Magnetic concentration parameters of bulk and size-fractionated samples from NPGP1302-1B. **(A)** Saturation isothermal remanent magnetization (SIRM); **(B)** anhysteretic remanent magnetization (ARM); **(C)** hard (>300 mT) IRM ($HIRM_{300}$); and **(D)** hard (>100 mT) IRM ($HIRM_{100}$). Values are mass-weighted by multiplying fractional abundance (%). For comparison, the bulk values from Shin et al. (2018) are shown as gray shaded area. Marine Isotope Stages (MIS) are labeled as numbers on the top. Volcanic ash layers at ~80 and ~270 ka are marked by orange bars.

the previous study (Shin et al., 2018). In addition, the relative significance composition of low and high coercivity minerals was estimated by comparison of S-ratios.

SIRM and ARM

SIRM values of the sized fractions display similar variations to bulk SIRM, showing markedly low values in all fractions during MIS 6, 8, and 10 (**Figure 2A**). Of the five fractions, the 2–8 μm fraction has relatively high SIRM values with the highest average PMC of 31% (**Figure 2A** and **Table 1**), revealing higher contribution (36–38%) during MIS 1 and 9, and lower contribution (19–27%) during MIS 7 and 8 (**Figure 3A**). The finest fraction (<2 μm) does not show distinctively high SIRM values (**Figure 2A**), and the average PMC (25%) is lower than the 2–8 μm fraction (**Table 1**). Although coarser fractions (8–31 and 31–63 μm) have slightly lower average PMC values of 21 and 22%, respectively (**Table 1**), they occasionally show significantly high SIRM values and PMC up to 43% (**Figures 2A**, **3A**). In particular, the 31–63 μm fraction exhibits the maximum SIRM values with PMC of 28–43% during MIS 7 and around a volcanic ash layer at ~270 ka (**Figures 2A**, **3A**). The coarsest fraction (>63 μm) contributes a small portion to the bulk SIRM

TABLE 1 | Percentage Magnetic Contribution (PMC) of each particle size fraction to bulk magnetic concentration parameters.

(μm)	(%)	SIRM	ARM	$HIRM_{300}$	$HIRM_{100}$
<2	Mean PMC (range)	25 (8–55)	44 (21–63)	26 (10–43)	18 (6–36)
2–8	Mean PMC (range)	31 (22–38)	33 (22–46)	27 (15–34)	28 (14–42)
8–31	Mean PMC (range)	21 (13–27)	11 (2–18)	24 (16–31)	25 (18–31)
31–63	Mean PMC (range)	22 (10–43)	10 (3–25)	22 (6–49)	27 (14–51)
>63	Mean PMC (range)	2 (0.2–6)	2 (0.1–13)	1 (0–3)	2 (0.2–4)

(**Figure 3A** and **Table 1**) and could reflect inclusions of magnetic grains in host minerals, such as silicates (e.g., Chang et al., 2016; Chen et al., 2017).

Fine fractions (<2 and 2–8 μm) have high ARM values (**Figure 2B**), which is consistent with ARM being more sensitive to the presence of finer magnetic grains. Their average PMC dominates the bulk ARM, accounting for 44 and 33%, respectively (**Table 1**). The two dominant fractions show opposing fluctuations in some periods (**Figure 2B**), which probably reflects fine magnetite of different origins (e.g., biogenic vs. detrital magnetite). ARM values of coarser fractions (8–31 and 31–63 μm), similarly, vary with those of the 2–8 μm fraction (**Figure 2B**), but their average PMC is generally as low as 11 and 10%, for 8–31 and 31–63 μm fractions, respectively (**Table 1**).

HIRMs and S-Ratios

Bulk $HIRM_{300}$ and $HIRM_{100}$ variations resemble that of SIRM, reflecting a similar input mechanism for both high and low coercivity minerals (**Figures 2C,D**). Of the measured parameters, the bulk $HIRM_{300}$ does not show a noticeable decrease during MIS 6, 8, and 10 (**Figure 2C**) since high coercivity minerals (e.g., hematite) are resistant to dissolutions (Roberts, 2015). Fine fractions of <2 and 2–8 μm have relatively constant $HIRM_{300}$ values (**Figure 2C**), with average PMC values of 26 and 27%, respectively (**Table 1**). The PMC generally increases during glacials (MIS 2, 6, 8, and 10) (**Figure 3C**). On the other hand, the coarser fractions, 8–31 and 31–63 μm, display a relatively large fluctuation in $HIRM_{300}$ values (**Figure 2C**) with average PMC values of 24 and 22%, respectively (**Table 1**). Strikingly, the coarse fractions dominate the bulk $HIRM_{300}$ with peak values in MIS 7, as in SIRM, showing PMC of 62–74% (**Figures 2C**, **3C**).

Compared to the bulk $HIRM_{300}$, $HIRM_{100}$ variation is more similar to SIRM variation (**Figures 2A,C,D**). However, the <2 μm fraction has relatively low $HIRM_{100}$ values, with an average PMC of 18% (**Figure 2D** and **Table 1**). Meanwhile, $HIRM_{100}$ values of coarser fractions of 8–31 and 31–63 μm dominate the bulk values (**Figure 2D**), showing average PMC values of 25 and 26%, respectively (**Table 1**). The PMC of the coarse fractions to $HIRM_{100}$, exhibiting ∼50–80% together, is distinctively higher than to other parameters (**Figure 3**).

The sized fractions have relatively constant S_{300} ratios in the range of ∼0.95–0.98, except for significant decreases during MIS 6, 8, and 10. This indicates the dominance of low coercivity minerals (<300 mT) in all fractions. As shown by relative fluctuations in SIRM instead of $HIRM_{300}$ (**Figure 4**), the S_{300} decreases during MIS 6, 8, and 10 are associated with a decrease in low coercivity minerals. The lowest S_{300} in the <2 μm fraction supports the preferential dissolution of fine magnetites (e.g., Roberts, 2015). S_{100} of the sized fractions, similarly, changes with S_{300}, showing decreases during MIS 6, 8, and 10. However, more distinctly, S_{100} is lower in the coarse fractions (8–31 and 31–63 μm), reflecting the greater contribution of high coercivity minerals (>100 mT). This is consistent with relatively high PMC to the bulk $HIRM_{100}$ in the coarse fractions (**Figures 3D**, **4A**).

SEM Observations

SEM photos of magnetic extracts for the <2 μm and 8–31 μm fractions of 231 ka (361 cm depth) in **Figure 5**. For the <2 μm fraction (**Figures 5A,B**), magnetic particles show various morphologies with frequent occurrences of subangular–euhedral and cuboidal shapes with smooth surfaces. EDS analysis reveals that most of the particles are identified as iron-oxides showing distinctive Fe and O peaks (**Supplementary Figure S2**). Most of <100 nm particles are observed as cuboidal iron-oxides aggregated each other (lower panels of **Supplementary Figure S2**). On the other hand, magnetic extracts for the 8–31 μm fraction show angular, irregular, and vesicular morphologies with 10–30 μm particle sizes (**Figures 5C,D**). Such typical morphologies are characteristics of volcanic ashes (e.g., Riley et al., 2003). Within large alumino-silicates composed mainly of Al, Ca, and Si, iron-oxides are observed as submicron sized inclusions (**Figure 5D** and **Supplementary Figure S3**). Notably, the iron-oxide inclusions also have Ti as a major element.

For comparison, magnetic extracts for a volcanic ash layer (275 ka, 470 cm depth) were observed (**Figures 5E,F**). As expected, all the particles observed show similar morphologies to those in the 8–31 μm fraction. Ti-rich iron-oxides occur in the large alumino-silicate host (**Supplementary Figure S4**). Such morphological and compositional similarities indicate that most of large particles (>8 μm) including iron-oxides are probably in volcanic origin.

DISCUSSION

Climate Dependence of Volcanic Fraction

For the past ∼500 kyr, terrigenous sediments of ODP 1209B site on the South High of the Shatsky Rise, where our study core was collected at ∼50 km away (**Figure 1**), have shown a bimodal particle size distribution, with modes of ∼4 and ∼20 μm accounting for ∼60–100% and ∼0–40% of the terrigenous fraction, respectively (Zhang et al., 2019). The major components of the 4 and 20 μm modes have been identified as eolian dust and volcanic materials, respectively, based on their Nd isotopic (ε_{Nd}) and geochemical (La-Sc-Th) compositions (Zhang et al., 2019). In the ODP 1209B core, ε_{Nd} varied systematically with relative proportion of two size modes, in which ε_{Nd} increased toward volcanic end member composition

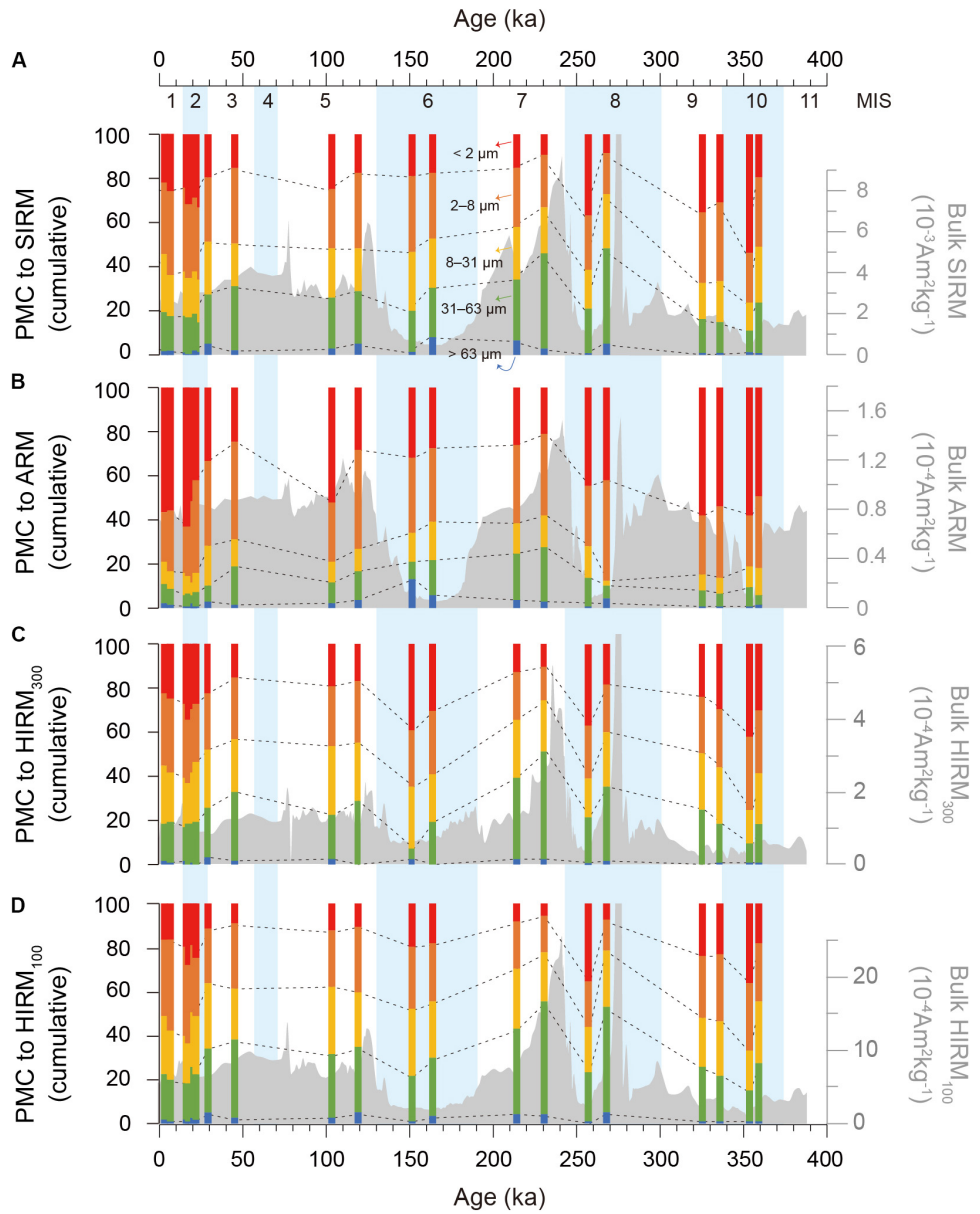

FIGURE 3 | Percentage magnetic contribution (PMC) of the size-fractionated samples to bulk magnetic parameters of **(A)** SIRM, **(B)** ARM, **(C)** $HIRM_{300}$, and **(D)** $HIRM_{100}$. PMC of each fraction is illustrated as cumulative bar chart. The color index is the same as in **Figure 2**.

with increasing proportion of 20 μm mode size fraction. The SEM observation results of our size-fractionated samples clearly confirmed the two main detrital origins, showing differences in morphologies of magnetic particles (**Figure 5**). Thus, the 2–8 and 8–31 μm samples of this study are expected to represent magnetic signals of the eolian and volcanic components, respectively. In addition, finer (<2 μm) and coarser (31–63 μm) fractions probably retain the extended magnetic properties of the two components.

SIRM reflects the total magnetic mineral concentration, and average PMC of fine fractions (<2 and 2–8 μm) dominantly contribute to the bulk values (**Table 1**). Given the dominant fine eolian component in the pelagic setting (Maher, 2011), it is natural that the fine fractions make a high magnetic contribution. However, coarse fractions (8–31 and 31–63 μm) show a significant PMC of >50% in some cases. For example, the coarse fractions in MIS 7 make up greater than 60% of bulk SIRM, with high mass-weighted SIRM values (**Figures 2A**, **3A**), implying significant contribution of volcanic particles to bulk magnetic concentration as confirmed by SEM observations (**Figures 5C,D**). Notably, the PMC of the coarse fractions is more distinctive in HIRMs than SIRM (**Figure 3** and **Table 1**).

Interestingly, the temporal change in the bulk SIRM and HIRMs shows positive correlations with PMCs of the coarse

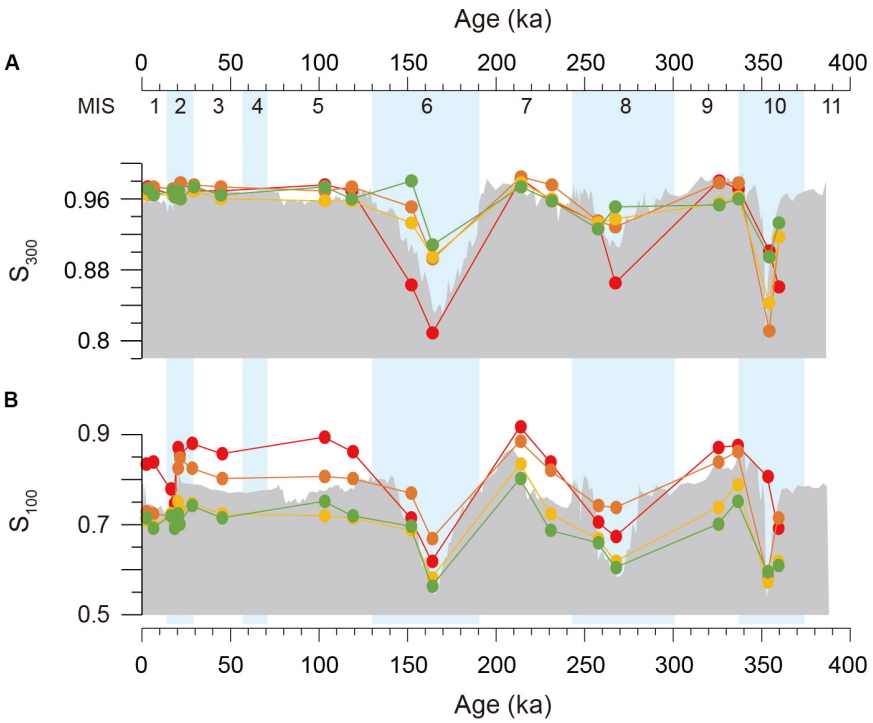

FIGURE 4 | (A) S_{300} and **(B)** S_{100} of bulk and size-fractionated samples. The lower S-ratios indicates greater contribution of high coercivity magnetic minerals. The color index is the same as in **Figure 2**.

fractions (8–31 and 31–63 μm), while the fine fractions (<2 and 2–8 μm) reveal negative correlations (**Figure 6**). Except for highly altered MIS 6, 8, and 10 samples that probably suffered magnetite dissolutions (Shin et al., 2018), PMC of the coarse fractions show a high correlation coefficient (r^2) of 0.87 for SIRM (**Figure 6A**). This strongly indicates that volcanic contribution has a close relationship with temporal changes of magnetic concentration. Such significance of volcanic contribution on magnetic signal is consistently found in the nearby core ODP site 1209B (**Figure 1**). As shown in **Figure 7**, Zhang et al. (2019) reported that relative changes in volcanic particle contribution of the ∼20 μm mode component at the site 1209B mimics the global oxygen isotope stack (LR04; Lisiecki and Raymo, 2005) during the last ∼500 kyr. When we compare this volcanic component with magnetic susceptibility from the site 1209B (Westerhold and Röhl, 2006), the two records show concurrent variations. This implies that volcanic particle contribution, rather than eolian dust, is the critical cause of the magnetic susceptibility variations. Moreover, the two records are very analogous to bulk magnetic susceptibility records of the studied core NPGP1302-1B (Shin et al., 2018) and a nearby core NGC102 (Yamamoto et al., 2007). Yamamoto et al. (2007) also stratigraphically correlated similar magnetic susceptibility changes of cores around the Shatsky Rise. All these consistent records indicate that bulk magnetic signals (i.e., magnetic mineral concentration) of northwest Pacific sediments sensitively responded to volcanic particle contribution.

As Zhang et al. (2019) suggested, the climate-dependence of volcanic particle contribution can be explained as the relative effect of dilution by evolving eolian dust flux, as dust input is enhanced during glacials (e.g., Hovan et al., 1991; Lambert et al., 2008; Jacobel et al., 2017); volcanic activities alone cannot directly paced to climate change. Of course, it should be noted that glacial magnetic signals represent the concentration of remaining magnetic minerals after magnetite dissolution (Shin et al., 2018). All particle fractions have low mass-concentration of magnetic minerals during MIS 6, 8, and 10 (**Supplementary Figure S1**) with low S-ratios (**Figure 4**), suggesting that magnetic minerals were primarily dissolved. Nevertheless, stronger contribution of eolian dust is likely well-reflected in higher PMC to $HIRM_{300}$ of fine fractions during glacials (**Figure 3**). Conclusively, our results provide a more comprehensive understanding of the cause of climate-dependent magnetic variations: volcanic coarse particles have strong potency to magnetic concentration parameters of both low and high coercivity minerals and thus acted as the main controller of bulk magnetic records in relation to terrigenous input. Volcanic materials, thus, should be considered as an essential factor for the interpretation of magnetic signals in the northwest Pacific, even though they account for a relatively small portion in sediments than dust.

Magnetic Characterization of the Volcanic Component

Magnetic properties of volcanic materials deposited in the northwest Pacific have been identified mostly from intercalated ash layers in bulk sediments. In general, the volcanic ash

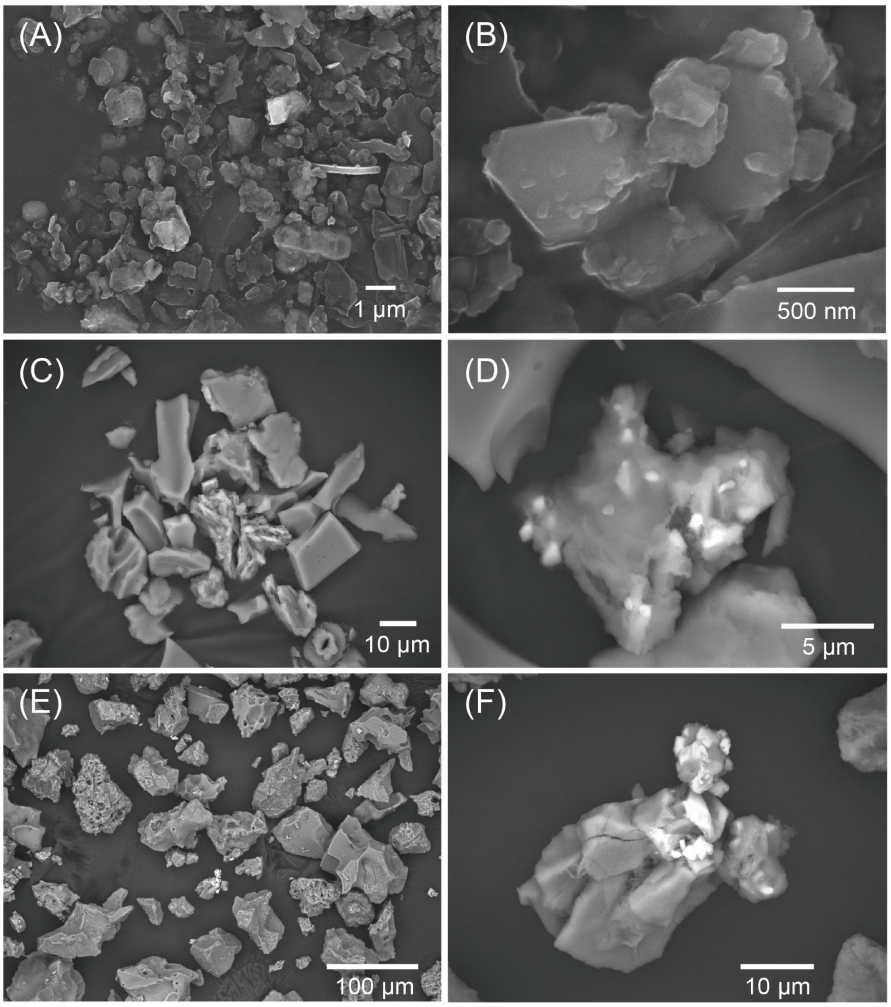

FIGURE 5 | Scanning electron microscopy (SEM) photos of magnetic extracts for **(A,B)** the <2 μm and **(C,D)** the 8–31 μm fractions of the 231 ka (361 cm depth) sample. **(E,F)** SEM photos for volcanic ash layer (275 ka, 470 cm depth) are presented for comparison. Representative chemical compositions are shown in **Supplementary Figures S2–S4**.

layers are characterized by magnetic spikes, associated with deposition of abundant magnetic minerals by short-term events (e.g., Yamamoto et al., 2007; Korff et al., 2016; Shin et al., 2018). Detailed magnetic analyses on the volcanic ash layers have also reported their magnetic features, such as rare antiferromagnetic minerals (Natland, 1993) and abundant ultrafine superparamagnetic particles (Bailey et al., 2011). In particular, Zhang et al. (2018) verified that volcanic ash layers deposited at a northern Pacific site (ODP site 885A; **Figure 1**) rarely contain pedogenic hematite and goethite, commonly present in eolian dust from arid regions, based on diffuse reflectance spectroscopy (DRS) signals. They also specified abundant high coercivity (80–100 mT) ferrimagnetic minerals in the ash layers from coercivity distribution. Along with these achievements, the particle size separation approach in this study can further provide magnetic information on the long-term airborne input of coarse volcanogenic particles in the northwest Pacific.

Considering the magnetic features of volcanic ash layers, coercivity distribution of fine (<2 and 2–8 μm) and coarse (8–31 and 31–63 μm) fractions could provide useful information on eolian- and volcanic-related magnetic signals, respectively. IRM component analysis for selected interglacial bulk samples and their sized fractions, avoiding glacial magnetic alteration, was performed (**Figure 8** and **Supplementary Figure S5**). Coercivity spectra of the four sized fractions are all dominated by component 2, with low coercivity ($B_{1/2}$ of 45–54 mT; **Figures 8C–F**). In the coercivity range, a narrow dispersion parameter (DP) of ∼0.2 in the finest fraction (<2 μm) is typical for biogenic magnetite, while wider DP in the other fractions corresponds to detrital magnetite (Egli, 2004; Yamazaki, 2009). Despite the dominant contribution of component 2, component 3, with a $B_{1/2}$ of 93–145 mT, is prominent in the coarse fractions with ∼22.5% contribution to SIRM (**Figures 6E,F**). On the other hand, component 4, which exhibits a higher coercivity ($B_{1/2}$ of 427–501 mT), is negligible in the coarse fractions.

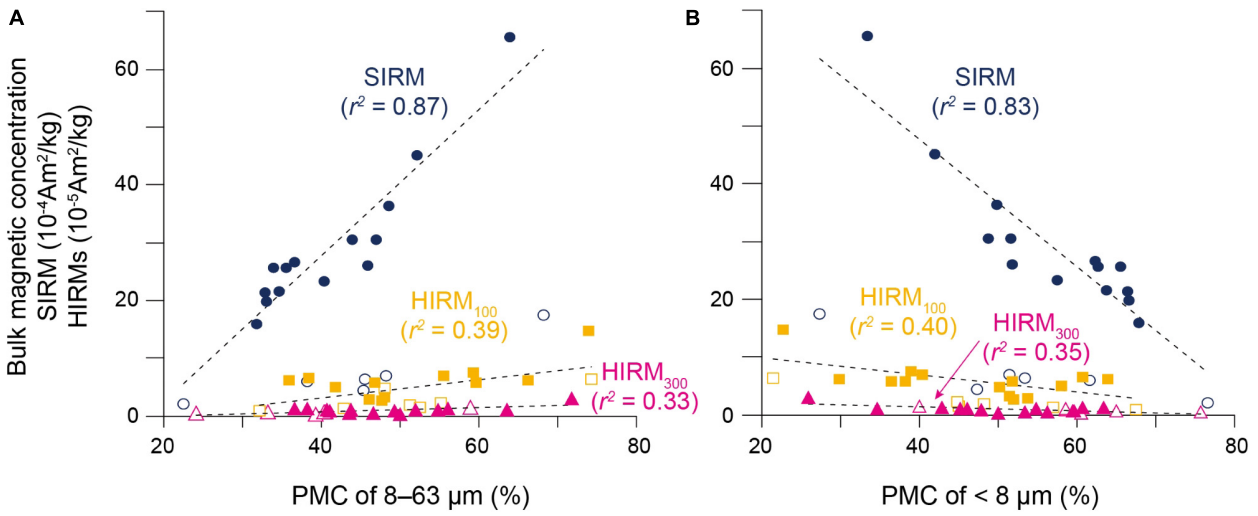

FIGURE 6 | Correlation between bulk magnetic concentration (SIRM, $HIRM_{300}$, and $HIRM_{100}$) and PMCs of **(A)** coarse (8–31 and 31–63 μm) and **(B)** fine (<2 and 2–8 μm) fractions. Glacial samples (MIS 6, 8, and 10), suspected to be altered (open symbols), were excepted for the correlation. PMCs of coarse and fine fractions reveal positive and negative correlations, respectively, with bulk concentration parameters.

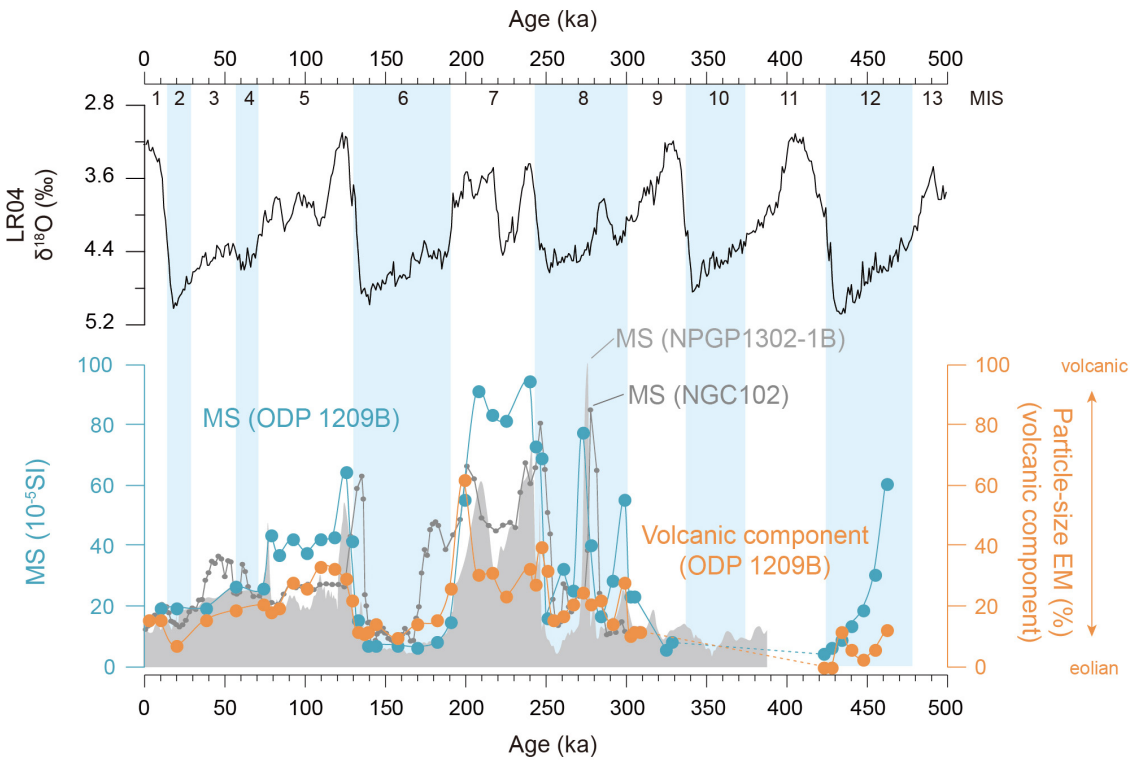

FIGURE 7 | Comparison of global oxygen isotope (LR04; Lisiecki and Raymo, 2005), magnetic susceptibility (MS) of ODP site 1209B (blue; Westerhold and Röhl, 2006; Bordiga et al., 2013 for age construction), particle size endmember (EM) contribution in ODP site 1209B (orange; Zhang et al., 2019), and MS records of NGC102 (dark gray; Yamamoto et al., 2007) and NPGP1302-1B (gray shaded; Shin et al., 2018). The EM corresponds to volcanic component relative to eolian dust in terrigenous fraction of ODP site 1209B.

In contrast, the fine fractions display high-field tails in the IRM acquisition curves (**Figure 8A**), indicating the presence of high coercivity antiferromagnetic minerals, such as hematite, in eolian dust. The high coercivity signal in the fine fractions could be useful to trace the eolian contribution as demonstrated using DRS parameters by Zhang et al. (2018). Taken together,

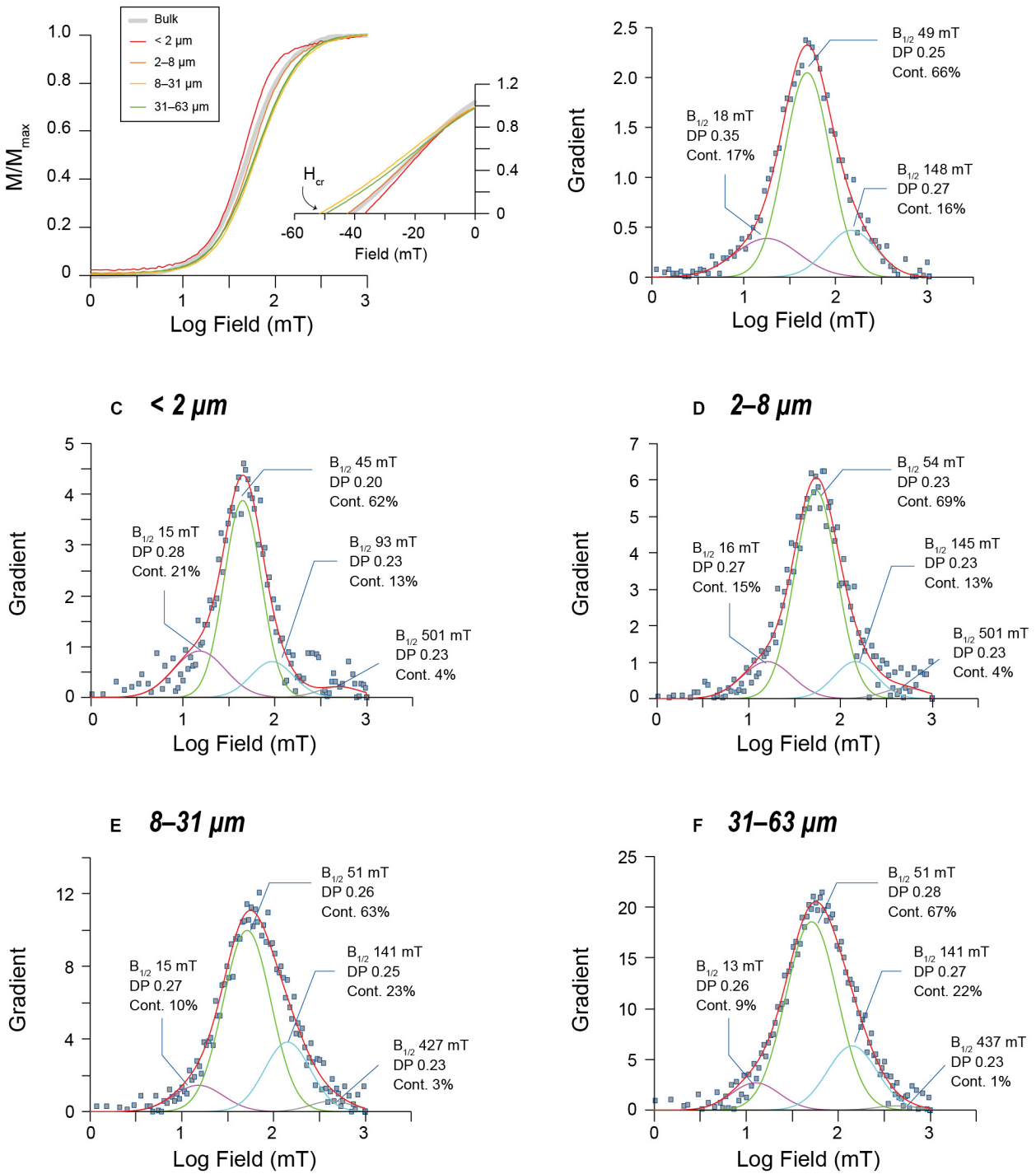

FIGURE 8 | Remanence acquisition and gradient plots for the 103 ka (164 cm depth) samples. **(A)** IRM acquisition and backfield decay curves for bulk and sized fractions altogether; **(B–F)** coercivity spectra of bulk and each sized fractions. In coercivity spectra, raw data points are indicated by squares; coercivity components are marked as purple (component 1), green (component 2), blue (component 3), and gray (component 4) lines; and sum of components are red lines fitted to the raw data. For each coercivity component, mean coercivity ($B_{1/2}$), dispersion parameters (DP), and contribution to SIRM (cont.%) are specified.

from the coercivity behaviors of the coarse fractions, volcanic materials can be characterized by abundant ferrimagnetic minerals of intermediate coercivity (∼100 mT). Although this coercivity range is slightly higher than the results from the ash layers originating from the Kamchatka-Aleutian arcs (i.e., the site 885A; Zhang et al., 2018), the coercivity distribution of our coarse fractions may be somewhat different depending on the relic of antiferromagnetic minerals in eolian dust (**Supplementary Figure S5**).

The IRM acquisition behavior of the bulk sample is similar to that of the 2–8 μm sample, particularly in the low coercivity range (**Figure 8A**). However, as shown in the bulk coercivity spectra (**Figure 8B**), the large dispersion of component 2 and the significant contribution of component 3 are more related to the coercivity distribution of the coarse fractions (**Figures 6E,F**). This confirms volcanic particles as an essential supply source of magnetic minerals. In particular, the abundant intermediate coercivity minerals (i.e., component 3) in volcanic particles can yield relatively high coercivity, as consistently presented by higher B_{cr} and lower S-ratios in the coarse fractions (**Figures 4**, **6A**, respectively). This implies that some proxies for higher coercivity fractions in bulk sediments (e.g., S-ratios and HIRMs) can be influenced by volcanic contribution. Thus, the use of such conventional eolian proxies for bulk sediments should be accompanied by consideration of volcanic contribution in coarse fraction in the northwest Pacific. In that respect, the magnetic analysis combined with particle size separation is a useful tool for characterizing volcanic and eolian contribution on bulk sediments.

CONCLUSION

Based on particle size-dependent magnetic properties, magnetic characteristics of volcanic materials and their contribution to bulk magnetic concentration was evaluated in ∼400 kyr sediments from the northwest Pacific. Magnetic properties of fine (<2 and 2–8 μm) and coarse (8–31 and 31–63 μm) fractions were isolated as eolian- and volcanic-related, respectively. SIRM and HIRMs ($HIRM_{300}$ and $HIRM_{100}$) were significantly contributed to by the coarse fractions, often showing >50% (up to 74%) of PMC. Moreover, the PMC of the coarse fractions generally varies in sync with the respective bulk values of SIRM and HIRMs, implying a close relationship between volcanic particle contribution and bulk magnetic concentration. Such a relationship is validated by covariation between magnetic susceptibility records and the relative proportion of volcanic components in the terrigenous fraction. Thus, we suggest volcanic materials as an important factor of magnetic concentration in the northwest Pacific, related to climate change. In addition, coercivity spectra of the coarse fractions reveal that volcanic materials contain abundant intermediate coercivity (∼100 mT) minerals, which can significantly influence high coercivity fraction parameters (e.g., S-ratios and HIRMs). Therefore, traditional coercivity proxies should be carefully interpreted in the northwest Pacific, in consideration with the volcanic contribution.

DATA AVAILABILITY STATEMENT

All datasets generated for this study are included in the article/**Supplementary Material**.

AUTHOR CONTRIBUTIONS

WK designed the sampling, reviewed the manuscript, and contributed to visualization and organization. JS designed the study, carried out analyses, and wrote the manuscript. KH contributed to the discussion. All authors contributed to the article and approved the submitted version.

FUNDING

This study was financially supported by the Ministry of Oceans and Fisheries (20160099) and the Korea Institute of Ocean Science and Technology (PE99824).

ACKNOWLEDGMENTS

We appreciate the editor MK for handling the paper and the two reviewers QL and BR for improving the manuscript significantly. We would like to thank Dr. S. J. Pak for his advice on SEM observations. IRM curves were acquired at the paleomagnetism laboratory of the Center for Advanced Marine Core Research (CMCR), Kochi University. We would like to thank Editage (http://www.editage.co.kr) for English language editing.

SUPPLEMENTARY MATERIAL

The Supplementary Material for this article can be found online at: https://www.frontiersin.org/articles/10.3389/feart.2020.00300/full#supplementary-material

REFERENCES

Atterberg, A. (1912). Die mechanische Bodenanalyse und die klassifikation der mineral böden sechwedens. *Int. Mitt. Bodenk.* 2, 312–342.

Bailey, I., Liu, Q., Swann, G. E. A., Jiang, Z., Sun, Y., Zhao, X., et al. (2011). Iron fertilisation and biogeochemical cycles in the sub-Arctic northwest Pacific during the late Pliocene intensification of northern hemisphere glaciation. *Earth Planet. Sci. Lett.* 307, 253–265. doi: 10.1016/j.epsl.2011.05.029

Bordiga, M., Beaufort, L., Cobianchi, M., Lupi, C., Mancin, N., Luciani, V., et al. (2013). Calcareous plankton and geochemistry from the ODP site 1209B in the NW Pacific Ocean (Shatsky Rise): new data to interpret calcite dissolution and paleoproductivity changes of the last 450ka. *Palaeogeogr. Palaeoclimatol. Palaeoecol.* 371, 93–108. doi: 10.1016/j.palaeo.2012.12.021

Bory, A. J. M., Biscaye, P. E., and Grousset, F. E. (2003). Two distinct seasonal Asian source regions for mineral dust deposited in Greenland (NorthGRIP). *Geophys. Res. Lett.* 30, 1–4. doi: 10.1029/2002GL016446

Chang, L., Roberts, A. P., Heslop, D., Hayashida, A., Li, J., Zhao, X., et al. (2016). Widespread occurrence of silicate-hosted magnetic mineral inclusions in marine sediments and their contribution to paleomagnetic recording. *J. Geophys. Res. Solid Earth* 121, 8415–8431. doi: 10.1002/2016JB013109

Chen, J., Li, G., Yang, J., Rao, W., Lu, H., Balsam, W., et al. (2007). Nd and Sr isotopic characteristics of Chinese deserts: implications for the provenances of Asian dust. *Geochim. Cosmochim. Acta* 71, 3904–3914. doi: 10.1016/j.gca.2007.04.033

Chen, L., Heslop, D., Roberts, A. P., Chang, L., Zhao, X., McGregor, H. V., et al. (2017). Remanence acquisition efficiency in biogenic and detrital magnetite and recording of geomagnetic paleointensity. *Geochem. Geophys. Geosyst.* 18, 1435–1450. doi: 10.1002/2016GC006753

Doh, S.-J., King, J. W., and Leinen, M. (1988). A rock-magnetic study of giant piston core LL44-GPC3 from the central North Pacific and its paleoceanographic implications. *Paleoceanography* 3, 89–111. doi: 10.1029/PA003i001p00089

Egli, R. (2004). Characterization of individual rock magnetic components by analysis of remanence curves, 1. unmixing natural sediments. *Stud. Geophys. Geod.* 48, 391–446. doi: 10.1023/B:SGEG.0000020839.45304.6d

Egli, R., Chen, A. P., Winklhofer, M., Kodama, K. P., and Horng, C.-S. (2010). Detection of noninteracting single domain particles using first-order reversal curve diagrams. *Geochem. Geophys. Geosyst.* 11:Q01Z11. doi: 10.1029/2009GC002916

Evans, M., and Heller, F. (2003). *Environmental Magnetism: Principles and Applications of Enviromagnetics*. Amsterdam: Elsevier.

Hatfield, R. (2014). Particle size-specific magnetic measurements as a tool for enhancing our understanding of the bulk magnetic properties of sediments. *Minerals* 4, 758–787. doi: 10.3390/min4040758

Hatfield, R. G., Stoner, J. S., Reilly, B. T., Tepley, F. J., Wheeler, B. H., and Housen, B. A. (2017). Grain size dependent magnetic discrimination of Iceland and South Greenland terrestrial sediments in the northern North Atlantic sediment record. *Earth Planet. Sci. Lett.* 474, 474–489. doi: 10.1016/j.epsl.2017.06.042

Heslop, D. (2015). Numerical strategies for magnetic mineral unmixing. *Earth Sci. Rev.* 150, 256–284. doi: 10.1016/j.earscirev.2015.07.007

Hovan, S. A., Rea, D. K., and Pisias, N. G. (1991). Late pleistocene continental climate and oceanic variability recorded in Northwest Pacific Sediments. *Paleoceanography* 6, 349–370. doi: 10.1029/91PA00559

Jacobel, A. W., McManus, J. F., Anderson, R. F., and Winckler, G. (2017). Climate-related response of dust flux to the central equatorial Pacific over the past 150 kyr. *Earth Planet. Sci. Lett.* 457, 160–172. doi: 10.1016/j.epsl.2016.09.042

Kars, M., Musgrave, R. J., Kodama, K., Jonas, A.-S., Bordiga, M., Ruebsam, W., et al. (2017). Impact of climate change on the magnetic mineral assemblage in marine sediments from Izu rear arc, NW Pacific Ocean, over the last 1 Myr. *Palaeogeogr. Palaeoclimatol. Palaeoecol.* 480, 53–69. doi: 10.1016/j.palaeo.2017.05.016

Korff, L., von Dobeneck, T., Frederichs, T., Kasten, S., Kuhn, G., Gersonde, R., et al. (2016). Cyclic magnetite dissolution in Pleistocene sediments of the abyssal northwest Pacific Ocean: evidence for glacial oxygen depletion and carbon trapping. *Paleoceanography* 31, 600–624. doi: 10.1002/2015PA002882

Kruiver, P. P., and Passier, H. F. (2001). Coercivity analysis of magnetic phases in sapropel S1 related to variations in redox conditions, including an investigation of the S ratio. *Geochem. Geophys. Geosyst.* 2:181. doi: 10.1029/2001GC000181

Lambert, F., Delmonte, B., Petit, J. R., Bigler, M., Kaufmann, P. R., Hutterli, M. A., et al. (2008). Dust-climate couplings over the past 800,000 years from the EPICA Dome C ice core. *Nature* 452, 616–619. doi: 10.1038/nature06763

Lisiecki, L. E., and Raymo, M. E. (2005). A Pliocene-Pleistocene stack of 57 globally distributed benthic $\delta^{18}O$ records. *Paleoceanography* 20:PA1003. doi: 10.1029/2004PA001071

Maher, B. A. (2011). The magnetic properties of Quaternary aeolian dusts and sediments, and their palaeoclimatic significance. *Aeolian Res.* 3, 87–144. doi: 10.1016/j.aeolia.2011.01.005

Nakai, S., Halliday, A. N., and Rea, D. K. (1993). Provenance of dust in the Pacific Ocean. *Earth Planet. Sci. Lett.* 119, 143–157. doi: 10.1016/0012-821X(93)90012-X

Natland, J. (1993). "Volcanic ash and pumice at shatsky rise: sources, mechanisms of transport, and bearing on atmospheric circulation," in *Proceedings of the Ocean Drilling Program, 132 Scientific Results*, (College Station, TX: Ocean Drilling Program), 57–66. doi: 10.2973/odp.proc.sr.132.301.1993

Pettke, T., Halliday, A. N., Hall, C. M., and Rea, D. K. (2000). Dust production and deposition in Asia and the north Pacific Ocean over the past 12 Myr. *Earth Planet. Sci. Lett.* 178, 397–413. doi: 10.1016/S0012-821X(00)00083-2

Razik, S., Dekkers, M. J., and von Dobeneck, T. (2014). How environmental magnetism can enhance the interpretational value of grain-size analysis: a time-slice study on sediment export to the NW African margin in Heinrich Stadial 1 and Mid Holocene. *Palaeogeogr. Palaeoclimatol. Palaeoecol.* 406, 33–48. doi: 10.1016/j.palaeo.2014.04.009

Rea, D. K., Snoeckx, H., and Joseph, L. H. (1998). Late Cenozoic Eolian deposition in the North Pacific: Asian drying, Tibetan uplift, and cooling of the northern hemisphere. *Paleoceanography* 13, 215–224. doi: 10.1029/98PA00123

Riley, C. M., Rose, W. I., and Bluth, G. J. S. (2003). Quantitative shape measurements of distal volcanic ash. *J. Geophys. Res. Solid Earth* 108, 1–15. doi: 10.1029/2001jb000818

Roberts, A. P. (2015). Magnetic mineral diagenesis. *Earth Sci. Rev.* 151, 1–47. doi: 10.1016/j.earscirev.2015.09.010

Roberts, A. P., Pike, C. R., and Verosub, K. L. (2000). First-order reversal curve diagrams: a new tool for characterizing the magnetic properties of natural samples. *J. Geophys. Res. Solid Earth* 105, 28461–28475. doi: 10.1029/2000JB900326

Serno, S., Winckler, G., Anderson, R. F., Hayes, C. T., McGee, D., Machalett, B., et al. (2014). Eolian dust input to the Subarctic North Pacific. *Earth Planet. Sci. Lett.* 387, 252–263. doi: 10.1016/j.epsl.2013.11.008

Shin, J. Y., Yu, Y., Seo, I., Hyeong, K., Lim, D., and Kim, W. (2018). Magnetic properties of deep−sea sediments from the North Pacific: a proxy of glacial deep−water ventilation. *Geochem. Geophys. Geosyst.* 19, 4433–4443. doi: 10.1029/2018GC007735

Urbat, M., and Pletsch, T. (2003). "Pleistocene deep-sea sediment in ODP hole 1149A, Nadezhda Basin: sources, alteration, and age controls (0–800 ka)," in *Proceedings of the Ocean Drilling Program, 185 Scientific Results*, (College Station, TX: Ocean Drilling Program), doi: 10.2973/odp.proc.sr.185.012.2003

Westerhold, T., and Röhl, U. (2006). "Data report: revised composite depth records for Shatsky rise sites 1209, 1210, and 1211," in *Proceedings of the Ocean Drilling Program, 198 Scientific Results*, (College Station, TX: Ocean Drilling Program), doi: 10.2973/odp.proc.sr.198.122.2006

Yamamoto, Y., Yamazaki, T., Kanamatsu, T., Ioka, N., and Mishima, T. (2007). Relative paleointensity stack during the last 250 kyr in the northwest Pacific. *J. Geophys. Res.* 112:B01104. doi: 10.1029/2006JB004477

Yamazaki, T. (1999). Relative paleointensity of the geomagnetic field during Brunhes Chron recorded in North Pacific deep-sea sediment cores: orbital influence? *Earth Planet. Sci. Lett.* 169, 23–35. doi: 10.1016/S0012-821X(99)00064-3

Yamazaki, T. (2009). Environmental magnetism of Pleistocene sediments in the North Pacific and Ontong-Java Plateau: temporal variations of detrital and biogenic components. *Geochem. Geophys. Geosyst.* 10:Q07Z04. doi: 10.1029/2009GC002413

Yamazaki, T., and Ioka, N. (1997). Environmental rock-magnetism of pelagic clay: implications for Asian eolian input to the North Pacific since the Pliocene. *Paleoceanography* 12, 111–124. doi: 10.1029/96PA02757

Zhang, Q., Liu, Q., Li, J., and Sun, Y. (2018). An integrated study of the Eolian dust in pelagic sediments from the North Pacific Ocean based on environmental magnetism, transmission electron microscopy, and diffuse reflectance spectroscopy. *J. Geophys. Res. Solid Earth* 123, 3358–3376. doi: 10.1002/2017JB014951

Zhang, W., Li, G., and Chen, J. (2019). The application of Neodymium isotope as a chronostratigraphic tool in North Pacific sediments. *Geol. Mag.* 157, 768–776. doi: 10.1017/S001675681900089X

Zhao, T. L., Gong, S. L., Zhang, X. Y., Blanchet, J.-P., McKendry, I. G., and Zhou, Z. J. (2006). A simulated climatology of Asian Dust Aerosol and its trans-pacific transport. Part I: mean climate and validation. *J. Clim.* 19, 88–103. doi: 10.1175/JCLI3605.1

Conflict of Interest: The authors declare that the research was conducted in the absence of any commercial or financial relationships that could be construed as a potential conflict of interest.